

Mask-induced polarization effects at high numerical aperture

Andrew Estroff
Yongfa Fan
Anatoly Bourov
Bruce Smith
 Rochester Institute of Technology
 Microelectronic Engineering
 82 Lomb Memorial Drive
 Rochester, New York 14623
 E-mail: ACE9411@rit.edu

Abstract. Degradation in image contrast becomes a concern at higher numerical apertures (NAs) due to mask-induced polarization effects. We study how different photomask materials (binary and attenuated phase shift), feature sizes and shapes, pitch values, duty ratios (line to space), and wavelengths effect the polarization of transmitted radiation. Rigorous coupled-wave analysis (RCWA) is used to simulate the polarization of radiation by the photomask. The results show that higher NA leads to greater polarization effects in all cases. Off-axis illumination increases polarization in one of the first orders, decreasing it in the other. Nonvertical sidewall angles and rounded corners can also impact polarization, but the wavelength of incident radiation has no effect on polarization effects at the same NA values. In general, materials with higher refractive indices and lower extinction coefficients tend to pass more of the TM polarization state, whereas materials with lower refractive indices and a relatively wider range of extinction coefficients pass more TE polarized radiation. These properties can provide new design considerations for the development of next-generation masking materials. © 2005 Society of Photo-Optical Instrumentation Engineers. [DOI: 10.1117/1.2037507]

Subject terms: photomask; polarization; immersion lithography; high numerical aperture; wire-grid polarizer.

Paper SS04153R received Nov. 4, 2004; revised manuscript received Feb. 25, 2005; accepted for publication Mar. 8, 2005; published online Aug. 26, 2005.

1 Introduction

Smaller device dimensions and increasing numerical apertures (NAs) cause polarization effects at the photomask to become a concern. Minimum pitch values (Λ) on a photomask approach

$$\Lambda_{\text{mask}} = \frac{\lambda M}{(\sigma + 1)NA}, \quad (1)$$

for a system with $M=1/m$, where m is the magnification of the lens. Assuming $M=4$ ($m=0.25$ for a $4\times$ reduction system), $NA=0.85$, and $\sigma=1.0$ for current generation tools, $\Lambda_{\text{mask}}=2.35\lambda$. Next-generation tools moving toward $NA=1.2$ will result in a minimum mask period of 1.67λ , at which point there can be more significant polarization effects contributed by the photomask.

TE polarization is defined as polarization perpendicular to the plane of incidence (POI); additionally, radiation polarized in the POI is referred to as TM polarized. This is shown in Figure 1. As NA increases, the angle of incidence at the wafer's surface becomes more oblique. For TE polarization, NA is not a concern since there is no decrease in image contrast due to increased angle of incidence, and image contrast remains 1, as shown by Eqs. (2) and (4), where $\delta=kx(\sin \theta)$. However, for TM polarization, as the angle of incidence approaches 45 deg, the image contrast decreases until it reaches zero at an angle of 45 deg, or 90 deg between two interfering beams¹ [Eqs. (3) and (4)]. Also, TE and TM polarized radiation states do not interfere

with one another. This clearly highlights the importance of incorporating polarization into lithography modeling and simulation.

$$I_{\text{TE}} = 2|E_1|^2(1 + \cos \delta), \quad (2)$$

$$I_{\text{TM}} = 2|E_1|^2[1 + (\cos \delta)(\cos 2\theta)], \quad (3)$$

$$\text{contrast} = \frac{I_{\text{max}} - I_{\text{min}}}{I_{\text{max}} + I_{\text{min}}}. \quad (4)$$

Traditional wire-grid polarizers enable the attenuation of the TE polarized radiation while allowing the TM state to

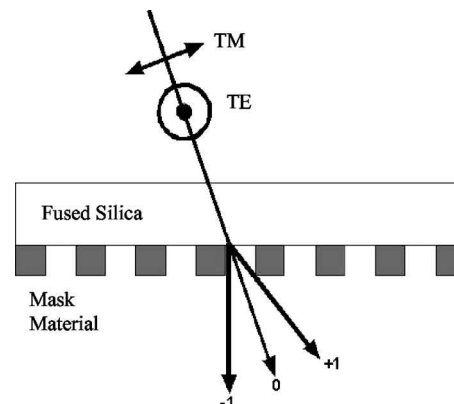


Fig. 1 Radiation incident upon photomask.

pass. The electric field of the TE polarized light induces a current in the length of the wires. Forward transmitted radiation is out of phase with the incident TE wave and exhibits greatly reduced intensity. The electric field of the TM polarized light is perpendicular to the wires, a dimension in which the wires are very narrow and restrict the motion of the electrons. Therefore, most of the TM radiation is transmitted unaffected.²

The parameters that impact the efficiency of a traditional wire-grid polarizer include period, duty cycle, thickness, shape, and material. The grating period is the most important of these parameters as it determines the minimum wavelength that can be polarized for a specific diffracted order, as shown in Eq. (5). As the period decreases, wires become closer together, making it easier for TE polarization to induce a current in the wires. Additionally, narrower wires restrict electron motion in the direction perpendicular to the wire even more, lessening the attenuation of the TM mode. Duty cycle is defined as the wire width divided by the period. Assuming a fixed period, if the duty cycle increases, so does the wire width, attenuating both the TE and TM polarizations more. Again, as in the case for decreasing period, a larger duty cycle will result in a more efficient TM polarizer. As grating thickness increases, the wires are able to generate more current, creating a more efficient polarizer. The shape of the wires also has an effect on the transmission and polarization efficiency. Nonvertical sidewalls and rounded edges cause a decrease in polarization efficiency, a benefit to the lithographer.²

The transition region of a wire-grid polarizer is defined as being between half to twice the wavelength of the incident radiation. Wood noticed a sharp decrease in transmission in this region in 1902; this phenomenon became known as Wood's anomalies.³ In 1907, Lord Rayleigh analyzed Wood's data and noted that for a specific wavelength (λ), period (Λ), material refractive index (n), and angle of incidence (θ), a higher diffracted order (m) emerges, as⁴

$$\lambda = \frac{\Lambda(n \pm \sin \theta)}{m}. \quad (5)$$

Another phenomenon that occurs in the transition region is the transmission of TE polarization as opposed to TM polarization. These have been studied by Honkanen et al.⁵ as well as others, and are referred to as inverse wire-grid polarizers.

Traditional wire-grid polarizer features are relatively large and are similar in size to the wavelength of light

Table 1 Cr-O-N stack composition, where layer 1 is closest to substrate, and layer 4 is the farthest from it.

	Cr-O-N Stack Composition (%)			
	Layer 1	Layer 2	Layer 3	Layer 4
Cr	90.00	18.90	9.45	0.00
CrN	10.00	2.10	1.05	0.00
CrO _x	0.00	79.00	89.50	100.00

incident on the polarizer; the wires approximate a planar metal surface. Inverse wire-grid polarizers utilize effects that occur in small metal clusters, thus the properties of metal clusters must be examined.

Clusters can be classified by their size. The feature sizes studied in this experiment would be classified as large clusters. There are two types of cluster size effects: intrinsic and extrinsic. Large clusters experience extrinsic size effects, such as collective electronic or lattice excitations known as Mie resonances.

The quasistatic regime is defined as the region in which the radius of the cluster is much less than the wavelength of the incident radiation. The application of electrostatics enables the response of a small metal sphere to an electric field to be determined. The conduction electrons are allowed to move due to the influence of external fields, whereas the positive charges are assumed to be fixed. The internal field can be represented as

$$E_i = E_o \frac{3\epsilon_m}{\epsilon(\omega) + 2\epsilon_m}, \quad (6)$$

where ϵ_m is the dielectric constant of the surrounding medium, which is 1 in this case. The static polarizability of a metal sphere can then be represented as

$$\alpha_{cl} = 4\pi\epsilon_o R^3, \quad (7)$$

where R is the radius of the sphere. The internal field shown in Eq. (6) experiences a resonance when $\epsilon(\omega) + 2 = \text{minimum}$. Thus, for a metal sphere, $\epsilon(\omega)$ must be -2 for resonance.⁶

Table 2 Cr-O-N stack data, where layer 1 is closest to substrate, and layer 4 is farthest from it.

	Layer 1		Layer 2		Layer 3		Layer 4	
	193 nm	248 nm						
n	0.8209	0.8863	1.5649	1.8142	1.6740	1.9734	1.7782	2.1260
k	1.1825	1.8700	0.4121	0.7391	0.3597	0.6584	0.3148	0.5918
Thickness (Å)	500	500	133	133	133	133	133	133

Table 3 APSM material composition, where the host materials are in bold and italics.

	TaN-Si ₃ N ₄		Si-Si ₃ N ₄		MoO ₃ -SiO ₂		Ta ₂ O ₅ -SiO ₂	
	TaN	Si ₃ N ₄	Si	Si ₃ N ₄	MoO ₃	SiO ₂	Ta ₂ O ₅	SiO ₂
157 nm	X	X	X	X	10.00%	90.00%	11.50%	88.50%
193 nm	17.00%	83.00%	9.00%	91.00%	30.00%	70.00%	X	X
248 nm	27.00%	73.00%	10.00%	90.00%	27.00%	73.00%	X	X

This resonance frequency can also be obtained by utilizing the Drude plasma frequency (ω_p) equation for free-electron metals, inserting the static polarizability, and using the Wigner-Seitz radius (r_s), yielding

$$\omega_1 = \left(\frac{q^2}{m_e 4\pi\epsilon_0 r_s^2} \right)^{1/2}, \quad (8)$$

where m_e is the mass of an electron, $r_s = R/N^{1/3}$, and N is the number of conduction electrons.⁶ This resonance angular frequency can be converted to a resonance wavelength by the relationship

$$\lambda = 2\pi \frac{hc}{\omega_1}. \quad (9)$$

The resonance frequency is the plasmon frequency.

The movement of the negative charges mentioned previously induces polarization charges at the cluster surface, determining this frequency. These conduction electrons form an oscillatory system; in bulk, they form a “relaxatory” system. This explains why inverse wire-grid polarizers pass TE polarization and not TM polarization. TE polarized light sees a quasi-infinitely long structure, thus it looks like bulk material. TM polarized light sees a small cluster, and induces a particle plasmon oscillation. For the proper wavelength, this plasmon can absorb almost all of the incident radiation.⁶

However, the feature sizes studied in this experiment do not strictly fall within the quasistatic region, nor are they spheres. Electrostatic theory can be extended to account for

spheroids, ellipsoids, and cylindrical geometries, but electrodynamic calculations (Mie theory) must be taken into account for larger cluster sizes. Mie theory includes phase retardation effects, as well as the excitation of multipolar oscillations not included in the quasistatic regime. Note that the plasmon resonance spectrum for arbitrarily shaped clusters is not yet known.⁷

The features on the photomask cannot be sufficiently approximated by assuming that they are a grating comprised of a thin metal film on a dielectric substrate. For feature sizes greater than twice the wavelength, a diffraction grating results with little to no polarization effects. For feature sizes less than half of the wavelength, the mask acts as a zero-order wire-grid polarizer. Between half and twice the wavelength is a transition region where the mask polarizes and diffracts the radiation, and can act as an inverse polarizer for some materials.

2 Approach

A binary Cr_xO_yN_z-on-glass mask was modeled using an effective media approximation from data collected on materials deposited via magnetron sputtering and characterized by means of ultraviolet variable angle spectroscopy⁸ (UV-VASE). The four-layer stack described in Tables 1 and 2 represents the graded Cr_xO_yN_z stack.

Attenuated phase-shifting mask (APSM) materials were also modeled. The APSM materials chosen were tantalum nitride in a silicon nitride host (TaN-Si₃N₄), molybdenum oxide in a silicon dioxide host (MoO₃-SiO₂), silicon in a silicon nitride host (Si-Si₃N₄), and tantalum oxide in a sili-

Table 4 APSM material data.

	Data for Pi Phase Shifting Materials							
	TaN-Si ₃ N ₄		Si-Si ₃ N ₄		MoO ₃ -SiO ₂			Ta ₂ O ₅ -SiO ₂
	193 nm	248 nm	193 nm	248 nm	157 nm	193 nm	248 nm	157 nm
<i>n</i>	2.5626	2.3833	2.4317	2.3482	1.6253	1.5891	1.6458	1.704
<i>k</i>	0.489	0.433	0.4462	0.4246	0.223	0.2117	0.2246	0.2468
Thickness (Å)	631	913	687	936	1262	1647	1932	1122
Percentage Transmission	9.88	10.37	10.4	10.35	9.8	9.69	10.28	10.02

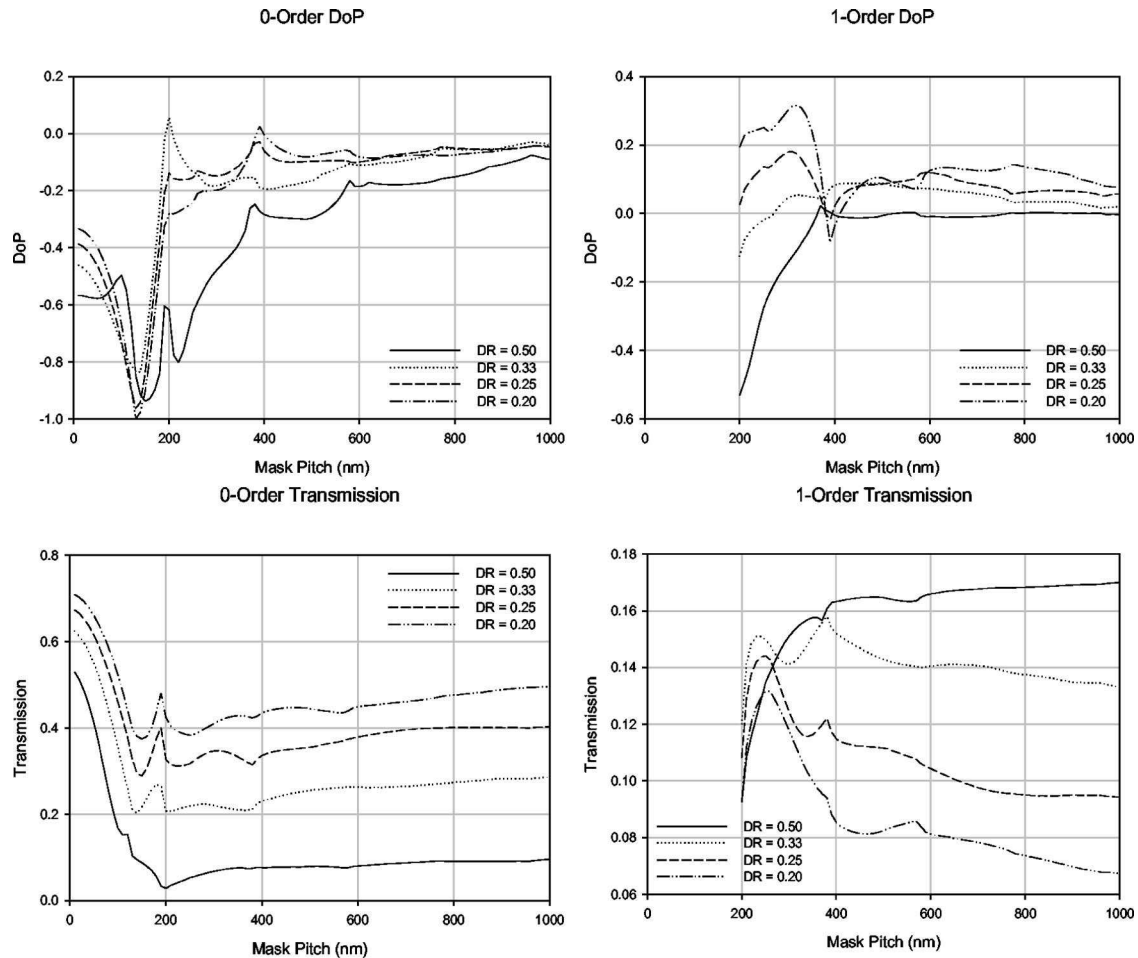


Fig. 2 Zero- and first-order DoP and transmission versus mask pitch for TaN-Si₃N₄.

con dioxide host (TaO₅-SiO₂). These materials were also modeled using the effective media approximation described earlier. All APSM films were designed for a π phase shift and 10% transmission. Tables 3 and 4 present the APSM material data.⁸

Rigorous coupled wave analysis (RCWA) provides an exact solution for Maxwell's equations. GSOLVER, a commercial software program capable of analyzing arbitrary grating thicknesses, numbers of materials, material indices of refraction, buried structures, and varied shapes (represented by stacked layers), was used to perform this experiment.⁹

Unpolarized radiation was modeled by first inputting a 100% TE polarized beam and measuring the transmitted TE intensity in the zeroth and first diffracted orders and then inputting a 100% TM polarized beam and measuring the transmitted TM intensity in the zeroth and first diffracted orders. This was done for 157-, 193-, and 248-nm radiation, depending on the mask material. The mask pitch was varied from 0 to 1000 nm (1 μ m) in 10-nm increments, and duty ratios examined were 0.2, 0.25, 0.33, and 0.5. Degree of polarization [Do; defined in Eq. (10)] was plotted versus mask pitch for the different materials, feature shapes, duty cycles, and wavelengths.

$$\text{DoP} = \frac{T_{\text{TE}} - T_{\text{TM}}}{T_{\text{TE}} + T_{\text{TM}}} \quad (10)$$

By this definition, a Do of -1 signifies fully TM polarized radiation, $+1$ signifies fully TE polarization, and 0 means equal TE and TM polarization. The plotted transmission is the average of the transmitted TE and TM polarization states.

The masks were simulated at all of the wavelengths listed for the specific material in Tables 2 and 4. All masks were simulated with the light incident at 0 deg, except for the binary mask, which was also simulated for an off axis illumination of NA=1.2 and $4\times$ reduction, which corresponds to 17.45 deg in air, and 11.5 deg in quartz. Additionally, all masks were simulated using rectangular features as well as triangular (equilateral) features.

3 Results

Wood's anomaly equation can be rearranged to provide the grating pitch at which a particular order emerges. For all on-axis cases in this experiment, this corresponds to the first order emerging at $\Lambda = \lambda$. At this point, the zero order in all cases experiences a decrease in transmission, and usually is also the mask pitch at which the zero order experi-

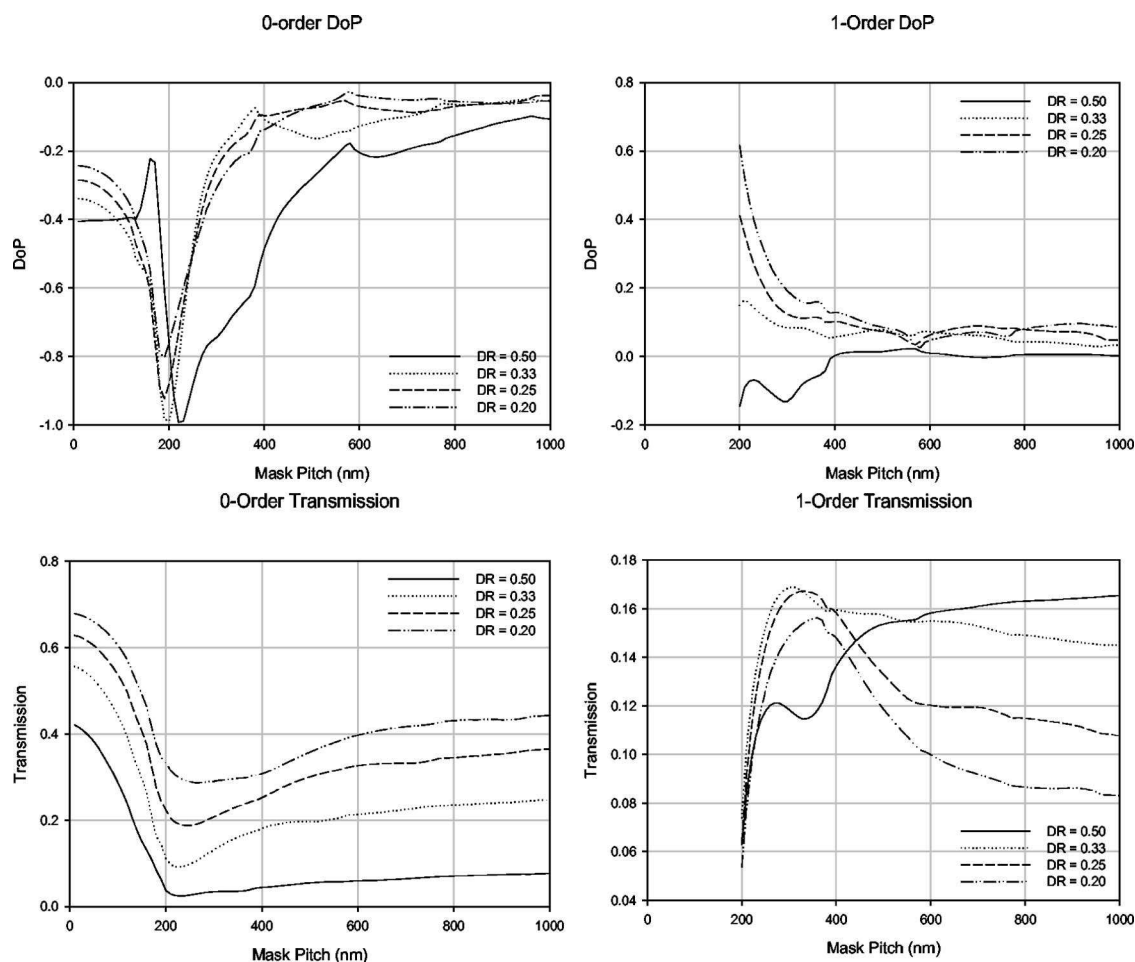


Fig. 3 Zero- and first-order DoP and transmission versus mask pitch for MoO₃-SiO₂.

ences the greatest polarization effects. Figures 2–4 show the degree of polarization and transmission data for rectangular shaped APSM and binary mask structures with on-axis illumination and varying duty ratio (TaN-Si₃N₄ and Si-Si₃N₄ are treated together due to similar results). All APSM materials act as traditional wire-grid polarizers for the zero order, and act as either traditional or inverse wire grid polarizers for the first order, depending on the duty ratio.

For TaN-Si₃N₄ and Si-Si₃N₄, decreasing duty ratio increases the TM polarization efficiency at $\Lambda = \lambda$ for the zero order, acting as a traditional wire-grid polarizer. The first-order behavior for these materials acts like a traditional wire-grid polarizer for equal lines and spaces, but like an inverse wire-grid polarizer for duty ratios less than 0.5. Transmission increases with decreasing duty ratio for the zero order, but decreases in the first order. This is consistent with basic Fourier analysis of a square-wave function. For MoO₃-SiO₂, as the duty ratio decreases, so does the TM polarization efficiency. At $\Lambda = \lambda$ for the zero order, there is a sharp decrease in polarization efficiency, and at slightly larger mask pitches there is a sharp increase; again the zero order acts as a traditional wire-grid polarizer. The first order acts as a weak traditional wire grid polarizer for a duty ratio of 0.5, but for decreasing duty ratios acts as a stronger inverse wire-grid polarizer. Transmission characteristics follow the same trend as in the other APSM case.

The binary Cr_xO_yN_z mask acts mainly as a traditional wire-grid polarizer for the zero order. Decreasing duty ratios lead to a decrease in the polarization efficiency of the zero order. Oppositely, the TE state is passed more than the TM state in the first orders, acting more like an inverse wire-grid polarizer, and decreasing duty ratio increases the polarization effects. The transmission follows the same trends as previously described.

Similarly to Figs. 2–4, degree of polarization was plotted versus mask pitch for 157 and 248-nm illumination. This was also performed for off-axis 193-nm illumination of the binary mask, and is shown in Fig. 5. The summary of these results for 1.2 and 0.85NA are shown in Fig. 6 for APSM and binary mask materials. It is observed that for the same NA, wavelength has no effect on the DoP for APSM materials, but for the binary mask materials, the zero order experiences a slight increase in DoP with increasing wavelength, whereas the first orders experience a slight decrease. Off-axis illumination (OAI) increases the DoP within one of the first orders, while decreasing the DoP within the other first order. A change in wavelength has a similar effect as the on-axis case, however, the first order, which experienced a decreased DoP previously, experiences an increase in the magnitude of DoP with an increase in wavelength.

The simulations that were run to generate Figs. 2–4

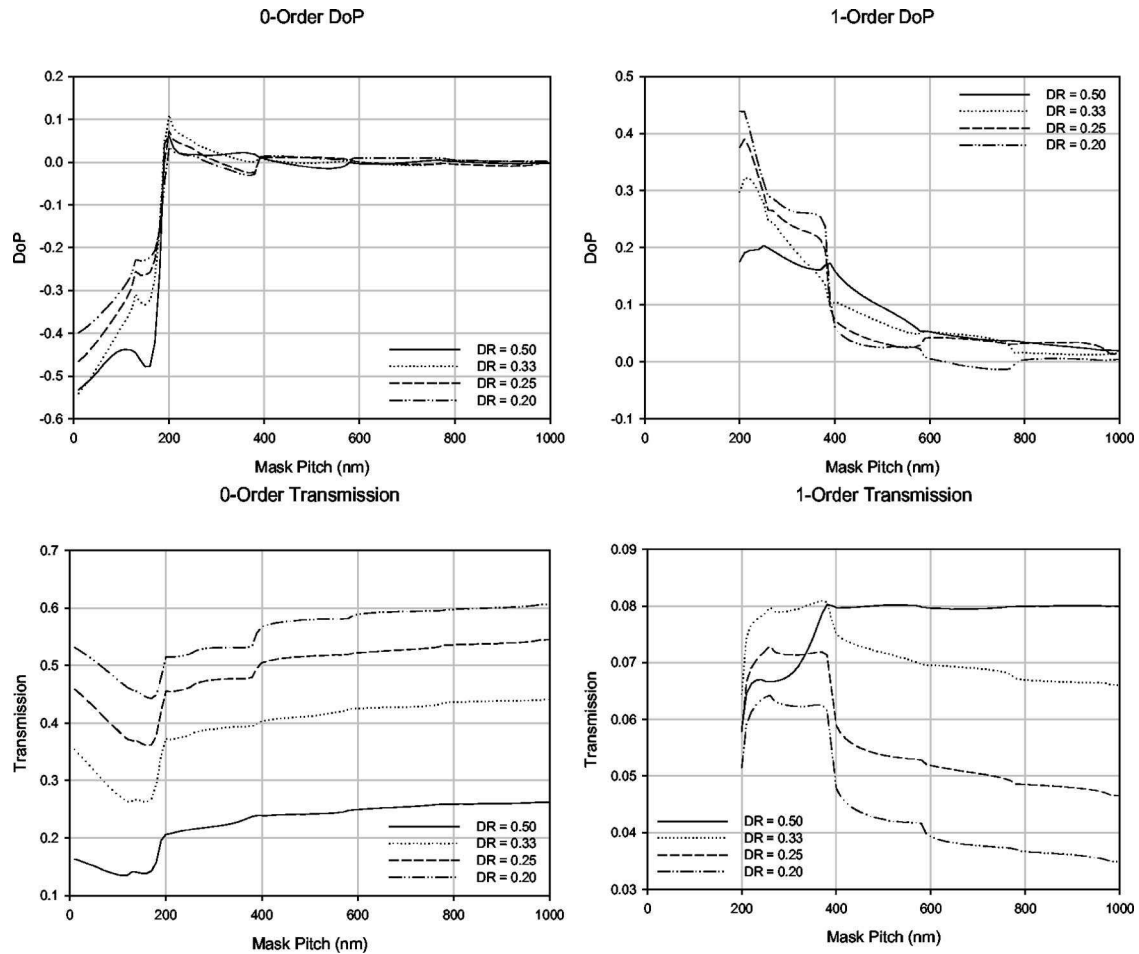


Fig. 4 Zero- and first-order DoP and transmission versus mask pitch for the binary $Cr_xO_yN_z$ mask.

were repeated for a 0.5 duty ratio for triangular-shaped features. The results are shown in Fig. 7. The sloped sidewalls have little effect on the DoP. At higher NAs, the DoP for APSM material features with sloped sidewalls is slightly less than that for the DoP of rectangular features. Sloped sidewalls have an opposite effect on the binary $Cr_xO_yN_z$

mask—the DoP is slightly greater than in the case of rectangular features. For all mask materials, the zero-order transmission for sloped sidewalls is greater than that for vertical sidewalls; the first-order transmission remains approximately the same.

In addition to the analysis of actual mask materials,

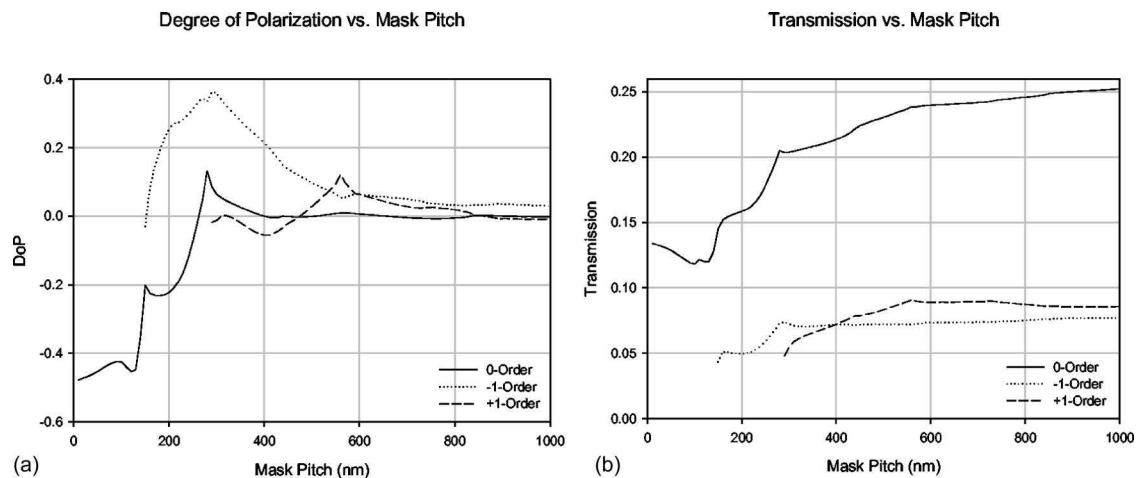


Fig. 5 Zero- and first-order (a) DoP and (b) transmission versus mask pitch for OAI of the binary $Cr_xO_yN_z$ mask.

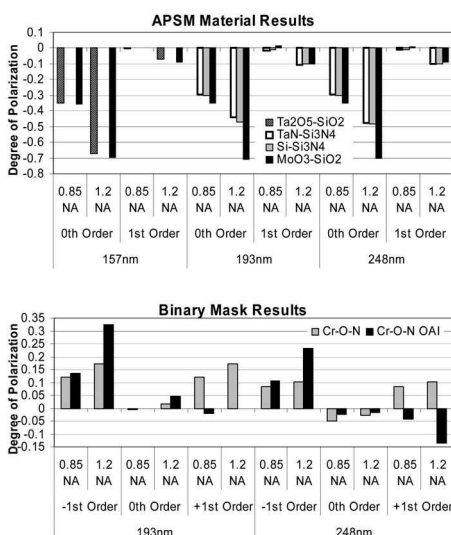


Fig. 6 APSM and binary mask material DoP for different wavelengths, illumination at different NAs.

simulations were performed to study the DoP as a function of n and k for π -phase shifting APSM materials. The index of refraction was varied from 0.5 to 3.0 (increments of 0.1) and the extinction coefficient from 0.0 to 1.0 (increments of 0.1). The thickness necessary to obtain a π -phase shift was calculated for a particular n and k value by first using Eq. (11) to calculate the interfacial phase jump at the substrate-mask material interface ($\Delta\Phi_{12}$), the mask material-air interface ($\Delta\Phi_{23}$), and the substrate-air interface ($\Delta\Phi_{13}$), and using¹⁰ these values in Eq. (12) to solve for d . A plot of APSM film thickness versus n and k is shown in Fig. 8. This thickness d was then used to calculate transmission^{10,11} as a function of n and k using Eq. (13). An extinction coefficient was found for a particular transmission and index of refraction, and lines were superimposed

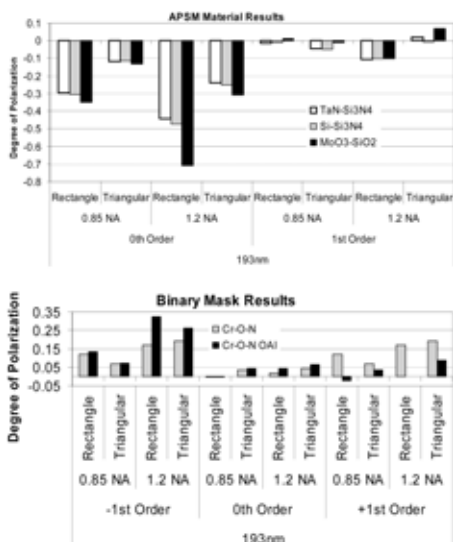


Fig. 7 APSM and binary mask material DoP for rectangular and pyramidal shapes at different NAs.

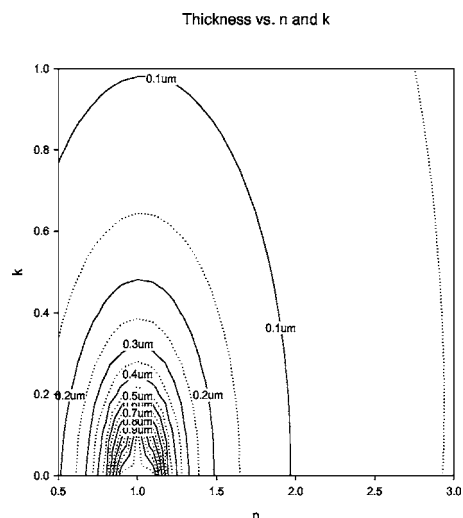


Fig. 8 Required APSM film thickness for π -phase shift plotted versus n and k (thickness in micrometers).

on the contour plot for 4 and 15% transmission. Figure 9 shows the contour plot of DoP versus n and k with transmission lines overlaid.

$$\Delta\Phi_{12} = \arg\left(\frac{2n_1^*}{n_1 + n_2^*}\right), \quad (11)$$

$$\Delta\Phi = \frac{2\pi}{\lambda}(n_2 - n_3)d + \Delta\Phi_{12} + \Delta\Phi_{23} - \Delta\Phi_{13}, \quad (12)$$

$$T(k) = \frac{(1 - R_{12})(1 - R_{23})}{1 - R_{13}} \exp\left(\frac{-4\pi}{\lambda}kd\right). \quad (13)$$

It is observed that materials with higher refractive indices and lower extinction coefficients tend to pass more of the TM polarization state. Materials with lower refractive indices and a relatively wider range of extinction coefficients pass more TE polarized radiation. Higher refractive index films are thinner than those with lower refractive indices.

Additionally, the APSM materials with transmission varying from 2 to 20% (2 to 70% for MoO₃-SiO₂) were superimposed on the contour plot to show viable candidates for next-generation mask materials. Materials that contribute more TE polarization effects or equal polarization weighting are desirable. From Fig. 9, materials that meet these criteria with a transmission between 4 and 15% have an index of refraction between 1.1 and 1.4, and an extinction coefficient between 0.05 and 0.2. None of the materials examined in this paper meet the desired polarization criteria.

4 Conclusion

RCWA was used to solve Maxwell's equations for photo-masks comprised of APSM materials and Cr_xO_yN_z. Different materials, radiation wavelengths, thicknesses, pitches, duty ratios, feature shapes, and incident angles all have an effect on how much a mask will polarize light.

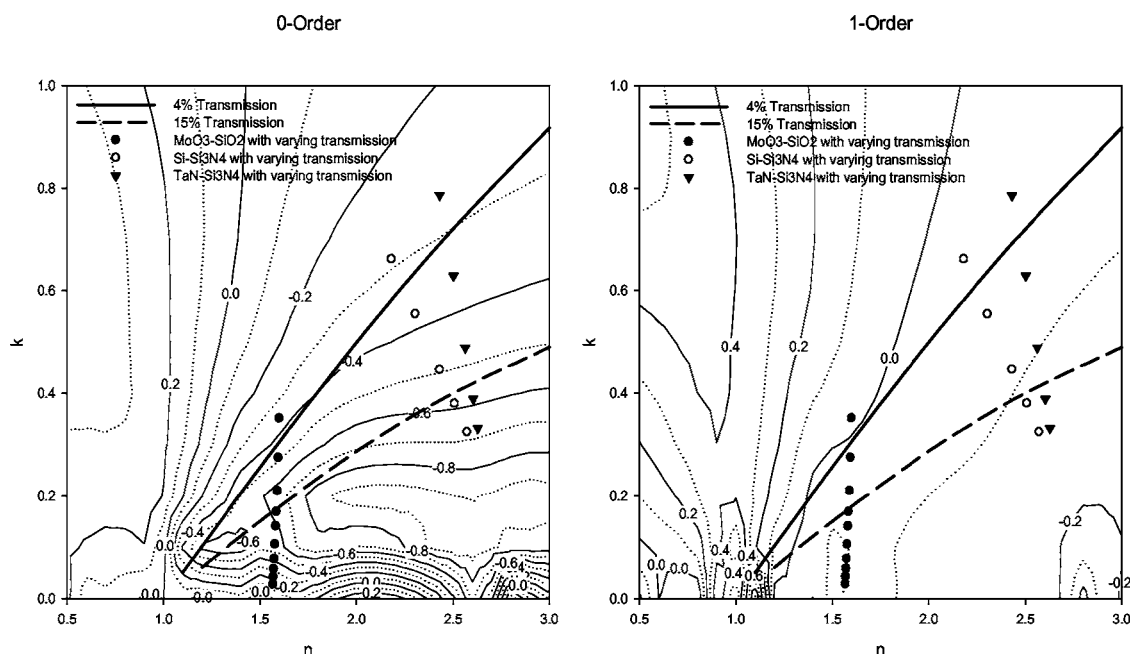


Fig. 9 DoP versus n and k .

All mask materials act predominantly as traditional wire-grid polarizers for the zero order, whereas different materials and duty ratios affect the polarization of the first diffracted orders differently. OAI causes an enhancement of the polarization effects in one of the first orders, and a decrease in the other. Sidewall angles other than 90 deg and rounded corners contribute little to the polarization of the incident radiation. The wavelength has virtually no effect on polarization effects at the same NA values.

Materials inducing a π -phase shift with higher refractive indices and lower extinction coefficients tend to pass more of the TM polarization state, whereas materials inducing a π -phase shift with lower refractive indices and a relatively wider range of extinction coefficients pass more TE polarization.

To reduce polarization effects, greater system reduction, resulting in larger mask feature sizes, could be used. Additionally, new mask materials could be researched.

References

1. D. Flagello, "Vector diffraction analysis of phase-mask imaging in photoresist imaging," *Proc. SPIE* **1927**, 395–412 (1993).

2. J. H. Johnson, "Wire grid polarizers for visible wavelengths," PhD Dissertation, University of Rochester, Rochester, NY (2003).
3. R. W. Wood, "Uneven distribution of light in a diffraction grating spectrum," *Philos. Mag.* **4**, 396–402 (Sep. 1902).
4. Lord Rayleigh, "On the remarkable case of diffraction spectra described by Prof. Wood," *Philos. Mag.* **14**, 60–65 (July 1907).
5. M. Honkanen, V. Kettunen, M. Kuitinen, J. Lautanen, J. Turunen, B. Schnabel, and F. Wyrowski, "Inverse metal-stripe polarizers," *Appl. Phys. B: Lasers Opt.* **68**, 81–85 (1999).
6. U. Kreibitz, *Optical Properties of Metal Clusters*, Springer, Berlin (1995).
7. O. J. F. Martin, Nanophotonics and Metrology Laboratory, Swiss Federal Institute of Technology, Lausanne, EPFL, <http://www.ifh.ee.ethz.ch/~martin/res50.en.html>.
8. RIT Materials Database, <http://www.microe.rit.edu/research/lithography/utilities.htm>.
9. GSOLVER Product Site, <http://www.gsolver.com>.
10. B. W. Smith, S. Butt, Z. Alam, S. Kurinec, and R L. Lane, "Attenuated phase shift mask materials for 248 and 193nm lithography," *J. Vac. Sci. Technol. B* **14**(6), 3719–3723 (1996).
11. A. Bourov, "Optical properties of materials for 157nm lithography," MS Thesis, Rochester Institute of Technology, Rochester, NY (2003).

Andrew Estroff is currently on assignment for Mentor Graphics at IMEC in Leuven, Belgium, and is pursuing his PhD in Microsystems Engineering at the Rochester Institute of Technology.

Biographies and photographs of the other authors not available.